Entanglement entropy of composite Fermi liquid states on the lattice: In support of the Widom formula

Ryan V. Mishmash and Olexei I. Motrunich
Department of Physics and Institute for Quantum Information and Matter, California Institute of Technology, Pasadena, CA 91125, USA and
Walter Burke Institute for Theoretical Physics, California Institute of Technology, Pasadena, CA 91125, USA
(Dated: May 31, 2016)

Quantum phases characterized by surfaces of gapless excitations are known to violate the otherwise ubiquitous boundary law of entanglement entropy in the form of a multiplicative log correction: $S \sim L^{d-1} \log L$. Using variational Monte Carlo, we calculate the second Rényi entropy for a model wavefunction of the $\nu = 1/2$ composite Fermi liquid (CFL) state defined on the two-dimensional triangular lattice. By carefully studying the scaling of the total Rényi entropy and, crucially, its contributions from the modulus and sign of the wavefunction on various finite-size geometries, we argue that the prefactor of the leading $L \log L$ term is equivalent to that in the analogous free fermion wavefunction. In contrast to the recent results of Shao et al. [PRL **114**, 206402 (2015)], we thus conclude that the "Widom formula" holds even in this non-Fermi liquid CFL state. More generally, our results further elucidate—and place on a more quantitative footing—the relationship between nontrivial wavefunction sign structure and $S \sim L \log L$ entanglement scaling in such highly entangled gapless phases.

The composite Fermi liquid (CFL) phase of the half-filled Landau level is a remarkable state of strongly interacting quantum matter. Electrons moving in two dimensions (2D) in the presence of a strong magnetic field will generically form gapped, incompressible quantum fluids [1, 2]; however, at densities corresponding to even denominator fractions (e.g., $\nu = 1/2$), the intriguing possibility of a gapless, compressible state arises [3]. Within the canonical picture [2, 4], here *composite fermions* consisting of one electron bound to two flux quanta feel *zero* effective magnetic field [3], thereby forming a metallic Fermi surface in spite of the extremely strong magnetic fields present. The CFL still stands today as the paradigmatic example of a strongly interacting gapless non-Fermi liquid state [3, 5–8], and it has very recently received an immense amount of exciting theoretical attention [9–20], refining the original theory of Halperin, Lee, and Read (HLR) [3].

In recent years, bipartite entanglement entropy (EE) has emerged as an indispensable tool in the study of quantum many-body states [22, 23]. It can reveal highly universal, even nonlocal, information about a quantum phase contained in a given ground state wavefunction. While EE has had remarkable success for gapped phases exhibiting topological order [24–27] and gapless Luttinger liquids [28–32], an interesting question concerns its ability to characterize two-dimensional (2D) highly entangled gapless systems in complicated situations such as the CFL, as well as simple ones such as the free Fermi gas with a sharp Fermi surface [see Fig. 1(a)].

These states are known to exhibit a multiplicative log violation of the boundary law:

$$S = \kappa\, L_A \log L_A\,, \tag{1}$$

with S the EE between a large real-space subregion of characteristic length L_A and its complement [see Fig. 1(c)-(d)]. For free fermions, the coefficient κ depends only on the *shapes* of the subregion and Fermi surface as given by an elegant geometric integral expression commonly referred to as the "Widom formula" [33–35]. In fact, κ is expected to be surprisingly universal and given by the Widom result even for an interacting Fermi liq-

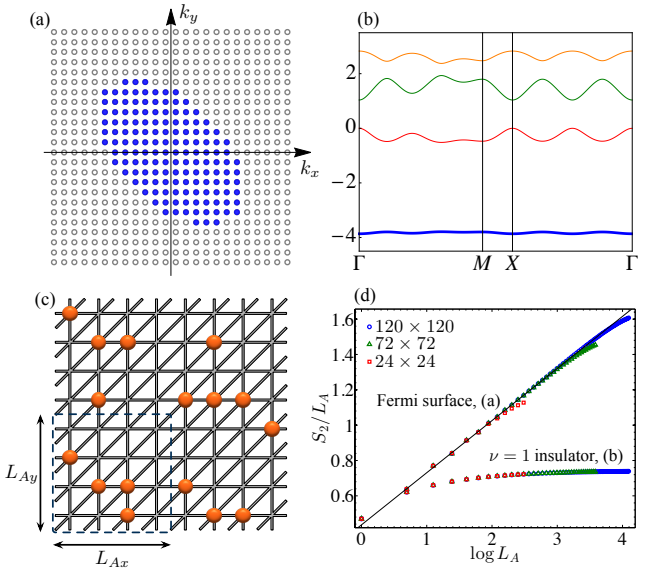

FIG. 1. (a) Filled Fermi sea with a sharp Fermi surface used to construct $\Psi_f^{\rm FS}$ on a 24×24 lattice with $N = 144$ electrons. (b) Band structure for $d_{1,2}$; the $\Psi_{d_{1,2}}^{(\nu=1)}$ Slater determinants are constructed by filling the lowest, nearly flat band (blue) which has Chern number $C = 1$. (c) We work on the 2D triangular lattice and consider subregions of size $L_{Ax} \times L_{Ay}$ for our calculations of S_2 [21]. (d) S_2 scaling for the free fermion states in (a) and (b) for $L_A \times L_A$ subregions embedded in various $L \times L$ systems (see legend); the black line indicates the Widom formula slope κ_W (see text).

uid [36–39], as well as for more exotic states with emergent surfaces of gapless excitations [40–42] which have the same Fermi surface content as the corresponding free Fermi gas. Loosely speaking, κ can thus generally be interpreted as measuring the "gaplessness" of the quantum state as contributed by the critical surface(s), emergent or otherwise [35, 37, 41–44].

Under the HLR construction [3], a model wavefunction for the CFL reads [45, 46]

$$\Psi_{\rm HLR}\left(\{\mathbf{r}_i\}\right) = \Psi_b^{(\nu=1/2)}\left(\{\mathbf{r}_i\}\right)\Psi_f^{\rm FS}\left(\{\mathbf{r}_i\}\right), \qquad (2)$$

where $\Psi_b^{(\nu=1/2)}$ is a Laughlin-type wavefunction for bosons at $\nu = 1/2$ [1, 47], $\Psi_f^{\rm FS}$ is a wavefunction for fermions in zero field exhibiting a Fermi surface (FS), and $\{\mathbf{r}_i\}$ are the coordinates of the N electrons at which both $\Psi_b^{(\nu=1/2)}$ and $\Psi_f^{\rm FS}$ are to be evaluated.

Recently, Ref. [48] presented a numerical study of the second Rényi entropy S_2 for a continuum wavefunction in the form of Eq. (2) projected into the lowest Landau level on a torus. These authors found that for square $L_A \times L_A$ subregions the prefactor κ in the leading $L_A \log L_A$ term of S_2 is approximately *twice* the corresponding Widom formula result, i.e., twice what is obtained for the zero-field free fermion wavefunction $\Psi_f^{\rm FS}$. This is a very striking result. Since $\Psi_b^{(\nu=1/2)}$ is a fully gapped state with a clear boundary law [26] (albeit a wavefunction with interesting structure of zeros and complex phases) and the Guztwiller projection implicit in Eq. (2) generally only tends to (slightly) decrease entanglement [29, 32, 40], such a dramatic increase in κ for this wavefunction is quite unexpected and deserving of further investigation.

Here, we study the entanglement entropy of analogous HLR-type wavefunctions on the lattice. Our wavefunctions are particularly easy to define and straightforward to handle using variational Monte Carlo [40, 49, 50], yet they should be in the same quantum phase as the state considered in Ref. [48]. We consider N spinless electrons moving on a toroidal 2D triangular lattice [see Fig. 1(c)] of dimension $L_x \times L_y$ with uniform magnetic flux penetrating the sample [51]. For concreteness, we take an electron density $\rho = N/(L_x L_y) = 1/4$ with $\pi/2$ external magnetic flux ($\hbar = c = e = 1$) per triangle, corresponding to one electron per two flux quanta, i.e., $\nu = 1/2$. To construct a model wavefunction for the HLR state in this system, we take $\Psi_b^{(\nu=1/2)}$ to be a Gutzwiller-projected product of two filled-Landau-level-like Slater determinants each at $\nu = 1$ [see Fig. 1(b)] and $\Psi_f^{\rm FS}$ to be a Slater determinant for the corresponding filled Fermi sea at zero field [see Fig. 1(a)]. The full wavefunction reads [21]

$$\Psi_{\rm HLR}^{\rm ferm}\left(\{\mathbf{r}_i\}\right) = \Psi_{d_1}^{(\nu=1)}\left(\{\mathbf{r}_i\}\right)\Psi_{d_2}^{(\nu=1)}\left(\{\mathbf{r}_i\}\right)\Psi_f^{\rm FS}\left(\{\mathbf{r}_i\}\right). \qquad (3)$$

Within a "parton" approach, this corresponds to decomposing the physical electron as $c = d_1 d_2 f$ subject to the constraint $d_1^\dagger d_1 = d_2^\dagger d_2 = f^\dagger f = c^\dagger c$ at each site. We will also briefly consider a bosonic analog of the HLR state appropriate for bosons at $\nu = 1$ [52, 53]. The construction parallels the fermionic state of Eq. (3) with a final wavefunction given by

$$\Psi_{\rm HLR}^{\rm bos}\left(\{\mathbf{r}_i\}\right) = \Psi_{d_1}^{(\nu=1)}\left(\{\mathbf{r}_i\}\right)\Psi_f^{\rm FS}\left(\{\mathbf{r}_i\}\right). \qquad (4)$$

As has now become standard, we compute the second Rényi entropy S_2 between a subregion A and the rest of the system by calculating the expectation value of the "swap" operator [40, 54]: $S_2 = -\log[{\rm Tr}(\rho_A^2)] = -\log\langle {\rm SWAP}_A\rangle$. Importantly, we employ the mod/sign decomposition first introduced in Ref. [40] to compute the total Rényi entropy as a sum of two terms: $S_2 = S_{2,\rm total} = S_{2,\rm mod} + S_{2,\rm sign}$ [55]. This not only enhances the efficiency of our Monte Carlo setup [21], but it is also central to our physical arguments below.

We begin by considering square $L_A \times L_A$ subregions embedded within total systems of size $L \times L$. The total Rényi entropy scaling for the free fermion state $\Psi_f^{\rm FS}$ on systems with $L = 24, 72, 120$ as calculated via the correlation matrix technique [56, 57] is shown in Fig. 1(d). Plotting S_2/L_A versus $\log L_A$ clearly reveals the multiplicative log violation. We fit the $L = 120$ data with L_A between 4 and 36 to obtain an accurate linear fit $S_2/L_A = \kappa \log L_A + a$ with $\kappa = \kappa_W \equiv 0.2950(6)$ and $a = 0.436(2)$. The fitted value κ_W is expected to be very close to that predicted by the Widom formula [34, 48]. The free fermion entropy for the gapped $d_{1,2}$ partons at $\nu = 1$ is also shown in Fig. 1(d); saturation to a boundary law is evident.

We now turn to Monte Carlo measurements of S_2 for the interacting model HLR wavefunctions given by Eqs. (3) and (4). We show in Fig. 2 calculations of $S_{2,\rm total}$ (left panel), $S_{2,\rm mod}$ (middle panel), and $S_{2,\rm sign}$ (right panel) for both the fermionic and bosonic HLR wavefunctions, as well as for the free fermion wavefunction, on a 24×24 system with $N = 144$ electrons. As is evident in the left panel of Fig. 2, the total entropy for the HLR wavefunctions indeed appears to have a slope κ significantly enhanced over the free fermion/Widom value [58]. For example, fits to the fermionic HLR data indicate a κ at least 60% larger than that obtained by similar fits to the free fermion data. We can thus corroborate the result of Ref. [48]: For square subregions with $O(100)$ electrons, the HLR wavefunction appears to violate the Widom formula by nearly a factor of two.

However, a closer inspection of the contributions from the modulus and sign of the wavefunctions, as shown in the middle and right panels of Fig. 2, reveals that this data is likely plagued by strong finite-size effects. The dramatic increase in entanglement for the HLR wavefunctions is almost entirely due to contributions from $S_{2,\rm mod}$ on these sizes, while $S_{2,\rm sign}$ is remarkably nearly equivalent for all three wavefunctions. However, $S_{2,\rm mod}$ displays

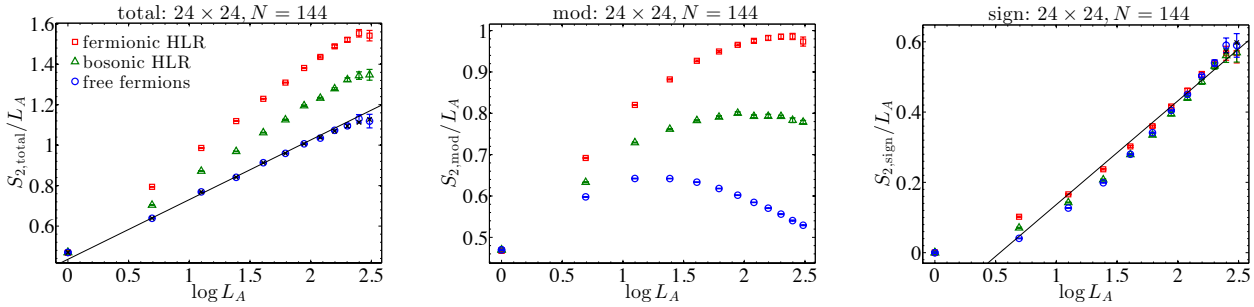

FIG. 2. Monte Carlo calculations of the total Rényi entropy (left panel) and the modulus (middle panel) and sign (right panel) components for the fermionic HLR, bosonic HLR, and free fermion wavefunctions on the $24\times24, N = 144$ system with $L_A \times L_A$ subregions. Here, and in Figs. 1(d) and 3, L_A ranges from 1 to $L/2$. The black "×" symbols indicate the exact S_2 values for free fermions from Fig. 1(d) (also present in Figs. 3 and 4), and the black lines indicate the Widom formula slope κ_W.

eventual boundary law behavior (with quite large boundary law coefficients for the HLR wavefunctions) [59]. On the other hand, it is clearly $S_{2,\text{sign}}$ which is ultimately responsible for the long-distance $L_A \log L_A$ scaling behavior [60]. Hence, in order to make conclusions about κ by analyzing only $S_{2,\text{total}}$, one should be deep in a regime of L_A where $S_{2,\text{mod}}$ has saturated to a boundary law.

While we are not yet in such a regime on the 24×24, $N = 144$ system [61], there are already telling indications in the $S_{2,\text{sign}}$ data that the HLR wavefunctions indeed obey the Widom formula. In the right panel of Fig. 2, we show a line with slope κ_W (intercept is arbitrary here and in Fig. 3). For L_A beyond just a couple lattice spacings, we see that $S_{2,\text{sign}}$ very nearly obeys the Widom formula for all three wavefunctions, perhaps most accurately for the fermionic HLR state itself. [The reason the slope for free fermions appears marginally larger is related to behavior in $S_{2,\text{mod}}$ (see above).] Finally, in Fig. 3 we show an alternative view of the fermionic HLR (left panel) and free fermion (right panel) data from Fig. 2, where we also include data from a smaller system: $16 \times 16, N = 64$. As in the right panel of Fig. 2, the black lines near the sign data indicate the Widom slope κ_W. The following three points are now obvious: (*i*) $S_{2,\text{mod}}$ for $\Psi_{\text{HLR}}^{\text{ferm}}$ indeed saturates to a boundary law; (*ii*) $S_{2,\text{sign}}$ for $\Psi_{\text{HLR}}^{\text{ferm}}$ is

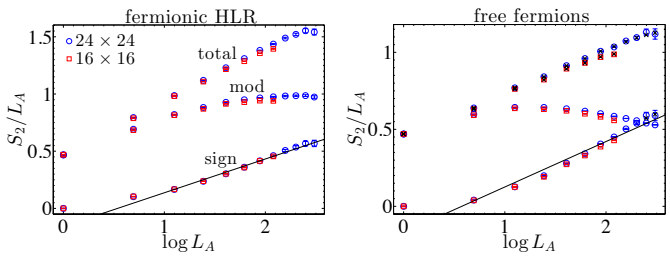

FIG. 3. Fermionic HLR (left panel) and free fermion (right panel) data for $24\times24, N = 144$ and $16\times16, N = 64$ showing $S_{2,\text{total}}$, $S_{2,\text{mod}}$, and $S_{2,\text{sign}}$ on the same axes.

well described by the Widom formula [62]; and (*iii*) the apparent Widom-formula violation in $S_{2,\text{total}}$ for $\Psi_{\text{HLR}}^{\text{ferm}}$ is mainly due to significant short-distance entanglement increase in the modulus of the wavefunction which results from strong correlations contained in the Jastrow-like factor $\left|\Psi_b^{(\nu=1/2)}\right|^2$ [63].

We now further bolster our arguments that the fermionic HLR state obeys the Widom formula by considering S_2 scaling on *strip* geometries. That is, we take $X \times L_y$ subregions embedded within $L_x \times L_y$ systems and vary X. In this case, for free fermions the Widom formula essentially reduces to the familiar quasi-1D form:

$$S_2(X, L_x) = \frac{c}{4} \log\left[\frac{L_x}{\pi} \sin\left(\frac{\pi X}{L_x}\right)\right] + A, \qquad (5)$$

where $c = N_{\text{slices}}$ is simply the number of "slices" through which the quantized k_y momenta pierce the Fermi surface, and we have used the familiar chord length ℓ inside the log [64] (appropriate for X comparable to L_x). More generally, at least in the quasi-1D limit ($L_x \gg L_y$), c is the *central charge* [28], i.e., the number of (nonchiral) gapless modes present in the realized multimode Luttinger liquid [29–32].

The narrowest nontrivial strip that we can consider has $L_y = 4$ [21] and $N_{\text{slices}} = 3$. For free fermions, we thus expect an effective central charge $c = N_{\text{slices}} = 3$. For the fermionic HLR state, on the other hand, we expect the Gutzwiller projection in Eq. (2) to *remove* one gapless mode [13, 29–31] giving $c = N_{\text{slices}} - 1 = 2$ (since $\Psi_b^{(\nu=1/2)}$ is fully gapped). Indeed we can unambiguously confirm this prediction on a $48 \times 4, N = 48$ system [see the $L_y = 4$ data in Fig. 5(a) and Fig. 6 in the Supplemental Material].

We have performed measurements on increasingly wide strips to approach the 2D limit. By performing fits to the data using Eq. (5), we can extract the central charge associated with the total entropy, denoted c_{total}, as well as contributions to the central charge from the mod and sign individually, denoted c_{mod} and c_{sign} (with $c_{\text{total}} =$

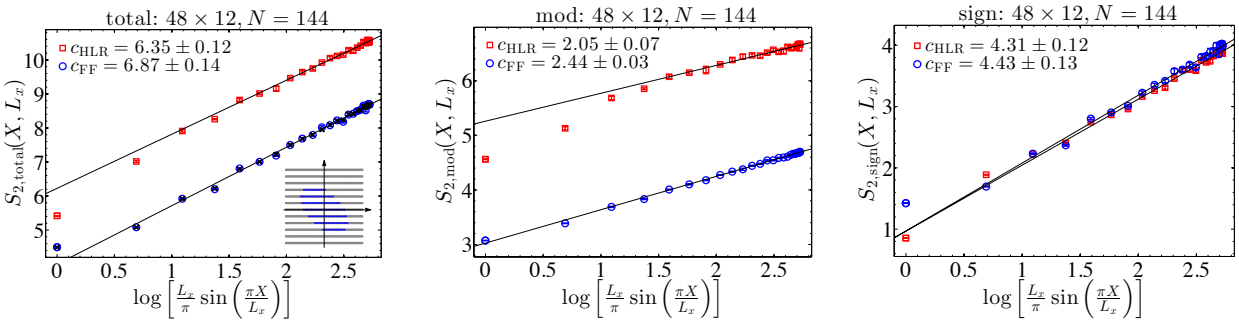

FIG. 4. From left to right, we show $S_{2,\text{total}}$, $S_{2,\text{mod}}$, and $S_{2,\text{sign}}$ versus $\log \ell$ on a $48 \times 12, N = 144$ system. The free fermion (FF) state has $N_{\text{slices}} = 7$ [see inset in the left panel; cf. Fig. 1(a)]. The lines correspond to fits to Eq. (5) with obtained values of c given in the legends [see Fig. 5(b) for corresponding fit parameters A].

$c_{\text{mod}} + c_{\text{sign}}$). Fig. 4 shows such data and the associated fits for $48 \times 12, N = 144$. This system has $N_{\text{slices}} = 7$, and indeed we find $c_{\text{total}} \approx 7$ for free fermions. For the HLR state, c_{total} is slightly reduced compared to free fermions but not quite precisely as $c = N_{\text{slices}} - 1$ (this is likely due to a combination of uncertainties in the fits and no longer being deep in the quasi-1D regime).

The middle and right panels of Fig. 4 again elucidate that it is $S_{2,\text{sign}}$ which is mainly responsible for the boundary law violation in these systems. Remarkably, the fermionic HLR and free fermion $S_{2,\text{sign}}$ results continue to basically collapse onto a single curve, both accurately following the scaling form Eq. (5). On the other hand, $S_{2,\text{mod}}$ grows relatively weakly with $\log \ell$ for both wavefunctions. In fact, the main qualitative difference between the two states is simply a larger intercept A in Eq. (5) for the HLR state, which is coming entirely from the modulus of the wavefunction; this is consistent with the data in Fig. 2. That is, the HLR state has an enhanced (nonuniversal) boundary law coefficient likely due to the significant short-distance entanglement present in the filled-Landau-level-like wavefunctions $\Psi_{d_{1,2}}^{(\nu=1)}$. However, this physics is clearly distinct from that giving rise to the multiplicative log boundary law violation.

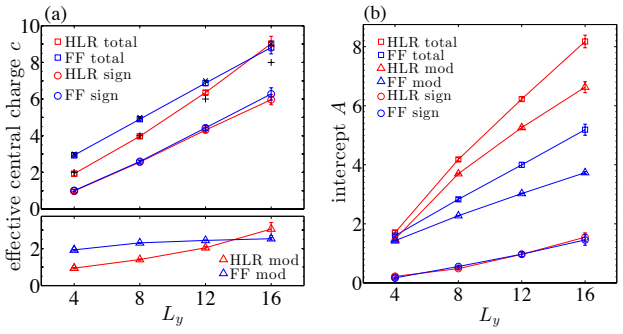

FIG. 5. (a) Central charge c and (b) intercept A fit parameters versus L_y for the fermionic HLR and free fermion (FF) wavefunctions on the strip geometry (lines are a guide to the eye). In (a), "×" and "+" symbols mark N_{slices} and $N_{\text{slices}} - 1$.

In Fig. 5, we summarize our strip geometry simulations for $L_y = 4, 8, 12$, and 16 with $L_x = 48, 48, 48$, and 36, respectively, all at $\rho = 1/4$. Fig. 5(a) shows the obtained central charge fit parameters c_{total}, c_{mod}, and c_{sign} for both the HLR and free fermion wavefunctions, while Fig. 5(b) shows the corresponding intercepts A [65]. We see in Fig. 5(a) that as L_y is increased, the *scaling* of the entropy becomes concentrated in c_{sign} for both states (cf. Fig. 2). All in all, there is no evidence of Widom formula violation in this data set, even in the total S_2 entropy itself. These results also put on firm footing the expression $c = N_{\text{slices}} - 1$ for the CFL used in the recent DMRG study of Ref. [13]. We have also performed simulations on a $24 \times 20, N = 120$ system with strip geometry subregions (see Fig. 6 in the the Supplemental Material). This system has nearly unit aspect ratio and is far from the quasi-1D limit. While due to convergence difficulties in $S_{2,\text{sign}}$ the data is not as clean as that in, e.g., Fig. 4, we still find the HLR and free fermion states to *scale* nearly equivalently with $c_{\text{total}} \approx 15$, $c_{\text{mod}} \approx 3$, and $c_{\text{sign}} \approx 12$ in both cases.

In conclusion, strongly motivated by the intriguing results of Ref. [48], we have analyzed in detail the Rényi entropy scaling for a model wavefunction of the composite Fermi liquid defined on the lattice. While our measurements of the total S_2 for square subregions appears to indicate a violation of the Widom formula in a manner similar to that in Ref. [48], we subsequently presented several arguments and lines of evidence that this is likely a strong finite-size effect, at least in our wavefunctions. It would be interesting to perform a similar analysis as we have here for the precise wavefunction considered in Ref. [48] (and also for the interacting Fermi liquid wavefunctions considered in Ref. [39]).

More generally, it is interesting to think about which types of wavefunctions may actually violate the Widom conjecture. On this note, we have also considered a wavefunction in the form of Eq. (2) but with $\Psi_b^{(\nu=1/2)} \rightarrow$

$\Psi_b^{(\nu=1/2)}/|\Psi_b^{(\nu=1/2)}|$. Such wavefunctions basically model attachment of flux at the mean-field level—as opposed to attachment of vortices in Eq. (2)—and are known to have various deficiencies [2, 4]. Interestingly, we find that $S_{2,\mathrm{sign}}$ for this wavefunction grows extremely quickly with L_A ($S_{2,\mathrm{mod}}$ is the same as for free fermions), and the full wavefunction may possibly have a scaling different from the Widom formula. We leave further investigation of this result for future work

For Gutzwiller-projected states containing multiple parton Fermi surfaces (see, e.g., Refs. [32, 66, 67]), we conjecture an effective Widom formula in which the total prefactor of $L_A \log L_A$ is approximately given by the sum of the κ_W prefactors for each Fermi surface individually. That is, since Gutzwiller projection seems to be relatively benign insofar as this physics is concerned, we expect to recover the mean-field result. This has already been shown to hold for the projected spinon Fermi surface state on the triangular lattice in Ref. [40]. However, Gutzwiller projection is known to only capture gauge fluctuations in a partial way [68]. Remedying this problem and subsequently studying the long-distance entanglement scaling of such wavefunctions constitutes an exciting and challenging future direction.

We gratefully acknowledge Sarang Gopalakrishnan, Max Metlitski, David Mross, Mike Mulligan, Sri Raghu, and Ashvin Vishwanath for valuable discussions. R.V.M. would like to thank Jim Garrison for explaining the second Monte Carlo scheme described in the Supplemental Material. This work was supported by the NSF through grant DMR-1206096 (O.I.M.); the Caltech Institute for Quantum Information and Matter, an NSF Physics Frontiers Center with support of the Gordon and Betty Moore Foundation; and the Walter Burke Institute for Theoretical Physics at Caltech. This work used the Extreme Science and Engineering Discovery Environment (XSEDE), which is supported by National Science Foundation grant number ACI-1053575.

[1] R. B. Laughlin, Phys. Rev. Lett. **50**, 1395 (1983).
[2] J. K. Jain, *Composite Fermions* (Cambridge University Press, 2007) Cambridge Books Online.
[3] B. I. Halperin, P. A. Lee, and N. Read, Phys. Rev. B **47**, 7312 (1993).
[4] J. Jain, Phys. Rev. Lett. **63**, 199 (1989).
[5] J. Polchinski, Nucl. Phys. B **422**, 617 (1994).
[6] C. Nayak and F. Wilczek, Nucl. Phys. B **417**, 359 (1994).
[7] C. Nayak and F. Wilczek, Nucl. Phys. B **430**, 534 (1994).
[8] B. L. Altshuler, L. B. Ioffe, and A. J. Millis, Phys. Rev. B **50**, 14048 (1994).
[9] D. T. Son, Phys. Rev. X **5**, 031027 (2015).
[10] C. Wang and T. Senthil, Phys. Rev. X **5**, 041031 (2015).
[11] M. A. Metlitski and A. Vishwanath, ArXiv e-prints (2015), arXiv:1505.05142 [cond-mat.str-el].
[12] C. Wang and T. Senthil, Phys. Rev. B **93**, 085110 (2016).
[13] S. D. Geraedts, M. P. Zaletel, R. S. K. Mong, M. A. Metlitski, A. Vishwanath, and O. I. Motrunich, Science **352**, 197 (2016), arXiv:1508.04140 [cond-mat.str-el].
[14] G. Murthy and R. Shankar, Phys. Rev. B **93**, 085405 (2016).
[15] S. Kachru, M. Mulligan, G. Torroba, and H. Wang, Phys. Rev. B **92**, 235105 (2015).
[16] M. Barkeshli, M. Mulligan, and M. P. A. Fisher, Phys. Rev. B **92**, 165125 (2015).
[17] D. F. Mross, J. Alicea, and O. I. Motrunich, ArXiv e-prints (2015), arXiv:1510.08455 [cond-mat.str-el].
[18] M. Mulligan, S. Raghu, and M. P. A. Fisher, ArXiv e-prints (2016), arXiv:1603.05656 [cond-mat.str-el].
[19] A. C. Balram and J. K. Jain, ArXiv e-prints (2016), arXiv:1604.03911 [cond-mat.str-el].
[20] C. Wang and T. Senthil, ArXiv e-prints (2016), arXiv:1604.06807 [cond-mat.str-el].
[21] See the Supplemental Material for details of our projected wavefunctions and Monte Carlo simulations.
[22] R. Horodecki, P. Horodecki, M. Horodecki, and K. Horodecki, Rev. Mod. Phys. **81**, 865 (2009).
[23] N. Laflorencie, ArXiv e-prints (2015), arXiv:1512.03388 [cond-mat.str-el].
[24] A. Kitaev and J. Preskill, Phys. Rev. Lett. **96**, 110404 (2006).
[25] M. Levin and X.-G. Wen, Phys. Rev. Lett. **96**, 110405 (2006).
[26] Y. Zhang, T. Grover, and A. Vishwanath, Phys. Rev. B **84**, 075128 (2011).
[27] Y. Zhang, T. Grover, A. Turner, M. Oshikawa, and A. Vishwanath, Phys. Rev. B **85**, 235151 (2012).
[28] P. Calabrese and J. Cardy, J. Stat. Mech. **2004**, P06002 (2004).
[29] D. N. Sheng, O. I. Motrunich, and M. P. A. Fisher, Phys. Rev. B **79**, 205112 (2009).
[30] M. S. Block, R. V. Mishmash, R. K. Kaul, D. N. Sheng, O. I. Motrunich, and M. P. A. Fisher, Phys. Rev. Lett. **106**, 046402 (2011).
[31] R. V. Mishmash, M. S. Block, R. K. Kaul, D. N. Sheng, O. I. Motrunich, and M. P. A. Fisher, Phys. Rev. B **84**, 245127 (2011).
[32] H.-C. Jiang, M. S. Block, R. V. Mishmash, J. R. Garrison, D. N. Sheng, O. I. Motrunich, and M. P. A. Fisher, Nature **493**, 39 (2013).
[33] D. Gioev and I. Klich, Phys. Rev. Lett. **96**, 100503 (2006).
[34] T. Barthel, M.-C. Chung, and U. Schollwöck, Phys. Rev. A **74**, 022329 (2006).
[35] B. Swingle, Phys. Rev. Lett. **105**, 050502 (2010).
[36] W. Ding, A. Seidel, and K. Yang, Phys. Rev. X **2**, 011012 (2012).
[37] B. Swingle, Phys. Rev. B **86**, 035116 (2012).
[38] B. Swingle, Phys. Rev. B **86**, 045109 (2012).
[39] J. McMinis and N. M. Tubman, Phys. Rev. B **87**, 081108 (2013).
[40] Y. Zhang, T. Grover, and A. Vishwanath, Phys. Rev. Lett. **107**, 067202 (2011).
[41] B. Swingle and T. Senthil, Phys. Rev. B **87**, 045123 (2013).
[42] B. Swingle, Phys. Rev. Lett. **111**, 100405 (2013).
[43] H.-H. Lai, K. Yang, and N. E. Bonesteel, Phys. Rev. Lett. **111**, 210402 (2013).
[44] H.-H. Lai and K. Yang, Phys. Rev. B **93**, 121109 (2016).
[45] E. H. Rezayi and F. D. M. Haldane, Phys. Rev. Lett. **84**,

4685 (2000).
[46] M. Barkeshli and J. McGreevy, Phys. Rev. B **86**, 075136 (2012).
[47] V. Kalmeyer and R. B. Laughlin, Phys. Rev. Lett. **59**, 2095 (1987).
[48] J. Shao, E.-A. Kim, F. D. M. Haldane, and E. H. Rezayi, Phys. Rev. Lett. **114**, 206402 (2015).
[49] D. Ceperley, G. V. Chester, and M. H. Kalos, Phys. Rev. B **16**, 3081 (1977).
[50] C. Gros, Annals of Physics **189**, 53 (1989).
[51] D. R. Hofstadter, Phys. Rev. B **14**, 2239 (1976).
[52] V. Pasquier and F. D. M. Haldane, Nuclear Physics B **516**, 719 (1998), cond-mat/9712169.
[53] N. Read, Phys. Rev. B **58**, 16262 (1998).
[54] M. B. Hastings, I. González, A. B. Kallin, and R. G. Melko, Phys. Rev. Lett. **104**, 157201 (2010).
[55] $S_{2,\mathrm{mod}}$ is the entropy of the modulus of the wavefunction, while $S_{2,\mathrm{sign}}$ is the component of the entropy due to non-trivial signs (phases). See the Supplemental Material for more details and discussion.
[56] I. Peschel, Journal of Physics A: Mathematical and General **36**, L205 (2003).
[57] I. Peschel and V. Eisler, Journal of Physics A: Mathematical and Theoretical **42**, 504003 (2009).
[58] The line shown in the left panel of Fig. 2 is the same as that in Fig. 1(d) with slope κ_W. It is not an independent fit over the 24×24 data, although the two match well.
[59] Note that when plotted this way $S_{2,\mathrm{mod}}/L_A$ for free fermions decreases slightly with $\log L_A$ beyond $L_A \approx 3$ on these sizes. This is likely due to subleading additive $\log L_A$ and/or constant terms in $S_{2,\mathrm{mod}}$; we expect it to eventually settle into a boundary law at large L_A though.
[60] Similar conclusions were also reached for the projected spinon Fermi surface wavefunction in Ref. [40].
[61] We expect that doubling L (i.e., 48×48, $N = 576$) may be sufficient, but such a system is well out of current computational abilities (also cf. Ref. [39]).
[62] Comparing the 16×16 and 24×24 data, $S_{2,\mathrm{sign}}/L_A$ appears to be well-converged in system size for $L_A = 1 - 8$.
[63] Even though the Jastrow potential is very long-range ($\sim -\log r$), we do not expect the entropy to increase stronger than boundary law since $S_{2,\mathrm{mod}} = S_{2,\mathrm{total}} - S_{2,\mathrm{sign}} \leq S_{2,\mathrm{total}}$ and $S_{2,\mathrm{total}}$ obeys a boundary law.
[64] H. Ju, A. B. Kallin, P. Fendley, M. B. Hastings, and R. G. Melko, Phys. Rev. B **85**, 165121 (2012).
[65] See the Supplemental Material for the full data sets (cf. Fig. 4) used to obtain these fits.
[66] O. I. Motrunich, Phys. Rev. B **72**, 045105 (2005).
[67] O. I. Motrunich and M. P. A. Fisher, Phys. Rev. B **75**, 235116 (2007).
[68] T. Tay and O. I. Motrunich, Phys. Rev. B **83**, 235122 (2011).
[69] J. McMinis, *Benchmark Studies Using Quantum Monte Carlo: Pressure Estimators, Energy, and Entanglement*, Ph.D. thesis, University of Illinois at Urbana-Champaign (2013).
[70] H. Shapourian and B. K. Clark, Phys. Rev. B **93**, 035125 (2016).

SUPPLEMENTAL MATERIAL

Details of the projected wavefunctions

The orbitals for the Slater determinants $\Psi_{a=d_1,d_2,f}$ used in Eqs. (3) and (4) of the main text are obtained by diagonalizing mean-field hopping Hamiltonians of the form

$$H_{\mathrm{MF}} = -\sum_{\mathbf{r}=(r_x,r_y)} \Big[t_{\hat{x}} e^{-i2r_y\phi} a^\dagger_{\mathbf{r}} a_{\mathbf{r}+\hat{x}} + t_{\hat{y}} a^\dagger_{\mathbf{r}} a_{\mathbf{r}+\hat{y}} + t_{\hat{x}+\hat{y}} e^{-i(2r_y+1)\phi} a^\dagger_{\mathbf{r}} a_{\mathbf{r}+\hat{x}+\hat{y}} + \mathrm{H.c.} \Big] \quad (6)$$

and filling the lowest N states. Throughout, we use a "squarized" version of the triangular lattice as shown in Fig. 1(c) with $r_x = 0, 1, \ldots, L_x - 1$ and $r_y = 0, 1, \ldots, L_y - 1$. Equation (6) corresponds to a Landau-like gauge giving uniform flux ϕ through each triangle.

At $\rho = 1/4$, we take $\phi = \pi/4$ for $d_{1,2}$ corresponding to $\nu = 1$ [see the filled nearly flat band in Fig. 1(b); there, $M = (\pi, \pi/4)$ and $X = (\pi, 0)$]. The magnetic unit cell for $d_{1,2}$ thus consists of four sites along a line in the y direction, which is very natural for our torus geometry. For the f partons, $\phi = 0$ [see the sharp Fermi surface in Fig. 1(a)].

We choose completely isotropic hopping patterns $t_{\hat{x}} = t_{\hat{y}} = t_{\hat{x}+\hat{y}} = 1$ for all partons except for the 48×12, $N = 144$ system in Figs. 4 and 5 of the main text, where we take $t_{\hat{x}} = t_{\hat{y}} = 1$ and $t_{\hat{x}+\hat{y}} = 1.01$ for the f partons to avoid degeneracies at the Fermi energy. The boundary conditions are taken to be periodic in the y direction for all partons and antiperiodic in the x direction for all partons except d_2; this produces a wavefunction with periodic boundary conditions in both directions.

Details of the Monte Carlo simulations

Given a wavefunction in coordinate space, $\phi(\alpha)$, the expectation value of the swap operator is given by [40, 54]

$$\langle \mathrm{SWAP}_A \rangle = \sum_{\alpha_1,\alpha_2} \frac{|\phi(\alpha_1)|^2}{\mathcal{N}} \frac{|\phi(\alpha_2)|^2}{\mathcal{N}} \left[\frac{\phi(\beta_1)\phi(\beta_2)}{\phi(\alpha_1)\phi(\alpha_2)} \right]. \quad (7)$$

Here $\alpha_1 = (a_1, b_1)$ and $\alpha_2 = (a_2, b_2)$ are configurations of the two copies 1 and 2 (a refers to degrees of freedom in subregion A, whereas b refers to degrees of freedom in the complement of A), while $\beta_1 = (a_2, b_1)$ and $\beta_2 = (a_1, b_2)$ are the swapped configurations, and $\mathcal{N} = \sum_\alpha |\phi(\alpha)|^2$ is the wavefunction normalization.

The mod/sign decomposition [40] is given by

$$\langle \mathrm{SWAP}_A \rangle = \langle \mathrm{SWAP}_{A,\mathrm{mod}} \rangle \langle \mathrm{SWAP}_{A,\mathrm{sign}} \rangle \tag{8}$$

$$\langle \mathrm{SWAP}_{A,\mathrm{mod}} \rangle = \sum_{\alpha_1,\alpha_2} \frac{|\phi(\alpha_1)|^2}{\mathcal{N}} \frac{|\phi(\alpha_2)|^2}{\mathcal{N}} \left| \frac{\phi(\beta_1)\phi(\beta_2)}{\phi(\alpha_1)\phi(\alpha_2)} \right|,$$

$$\langle \mathrm{SWAP}_{A,\mathrm{sign}} \rangle = \sum_{\alpha_1,\alpha_2} \frac{|\phi(\alpha_1)\phi(\alpha_2)\phi(\beta_1)\phi(\beta_2)|}{\mathcal{M}} e^{i\theta(\alpha_1,\alpha_2)},$$

where $\theta(\alpha_1,\alpha_2) = \arg[\phi^*(\alpha_1)\phi^*(\alpha_2)\phi(\beta_1)\phi(\beta_2)]$ and $\mathcal{M} = \sum_{\alpha_1,\alpha_2} |\phi(\alpha_1)\phi(\alpha_2)\phi(\beta_1)\phi(\beta_2)|$. Hence, $S_2 = S_{2,\mathrm{total}} = S_{2,\mathrm{mod}} + S_{2,\mathrm{sign}}$, with $S_{2,\mathrm{mod/sign}} = -\log\langle \mathrm{SWAP}_{A,\mathrm{mod/sign}} \rangle$.

Since $\langle \mathrm{SWAP}_{A,\mathrm{mod}} \rangle$ is the swap operator evaluated for the modulus of the wavefunction in this basis, i.e., $|\phi(\alpha)|$, $S_{2,\mathrm{mod}}$ is the entropy of the wavefunction $|\phi(\alpha)|$. On the other hand, $S_{2,\mathrm{sign}}$ can be interpreted as the component of the entropy *as a result of* nontrivial signs in the wavefunction: For a positive wavefunction, most notably $|\phi(\alpha)|$, $S_{2,\mathrm{sign}} = 0$ vanishes identically. [Note that $S_{2,\mathrm{sign}}$ is *not* simply the entropy obtained after taking the sign of the wavefunction $\phi(\alpha) \to \phi(\alpha)/|\phi(\alpha)|$.]

For systems with a globally conserved $U(1)$ symmetry—such as particle number conservation present in the wavefunctions in this work—it affords to be smart when performing the Monte Carlo walks in Eq. (8): Only configurations for which the total subregion occupations N_A in the two copies are identical [i.e., $N_A(\alpha_1) = N_A(\alpha_2) = n_A$] give nonzero contributions. [If $N_A(\alpha_1) \neq N_A(\alpha_2)$, then $\phi(\beta_1) = \phi(\beta_2) = 0$.] We have implemented two schemes for sampling $\langle \mathrm{SWAP}_A \rangle$, both of which allow the mod/sign factorization described above and which take advantage of the global particle number conservation (see also, e.g., Refs. [39, 69, 70] for similar schemes).

The first is the "particle number trick" explained in Ref. [48], which we briefly review. In this case, we decompose the final measurement as a sum over the possible subregion particle occupation numbers n_A:

$$\langle \mathrm{SWAP}_A \rangle = \sum_{n_A} (P_{n_A})^2 \langle \mathrm{SWAP}_{A,\mathrm{mod}} \rangle_{n_A} \langle \mathrm{SWAP}_{A,\mathrm{sign}} \rangle_{n_A} \tag{9}$$

Here, $\langle \mathrm{SWAP}_{A,\mathrm{mod/sign}} \rangle_{n_A}$ are the mod/sign measurements restricted to the subspace with n_A particles in subregion A for both copies. [Formally, one just replaces all sums in the expressions in Eq. (8)—including those in the normalizations $\mathcal{N}$ and $\mathcal{M}$—with sums over the restricted subspace: $\sum_{\alpha_1,\alpha_2} \to \sum_{\alpha_1,\alpha_2 \in n_A} \equiv \sum_{\alpha_1,\alpha_2} \delta_{N_A(\alpha_1),n_A} \delta_{N_A(\alpha_2),n_A}$.] The quantities P_{n_A} are simply the probabilities of finding n_A particles in subregion A for a single copy of the wavefunction,

$$P_{n_A} = \sum_{\alpha \in n_A} \frac{|\phi(\alpha)|^2}{\mathcal{N}} = \sum_{\alpha} \frac{|\phi(\alpha)|^2}{\mathcal{N}} \delta_{N_A(\alpha),n_A}, \tag{10}$$

and are obtainable in a straightforward single-copy simulation. In this scheme, we run separate swap simulations for each n_A and compile the results according to Eq. (9). Note that $\langle \mathrm{SWAP}_{A,\mathrm{mod}} \rangle$ in Eq. (8) can be computed by performing the sum in Eq. (9) with $\langle \mathrm{SWAP}_{A,\mathrm{sign}} \rangle_{n_A} = 1$; thus, the scheme readily gives both $S_{2,\mathrm{mod}}$ and $S_{2,\mathrm{sign}} = S_{2,\mathrm{total}} - S_{2,\mathrm{mod}}$.

The second method is similar to the original decomposition in Eq. (8), except that for both the mod and sign walks we only consider in our move scheme "swappable" configurations, i.e., those with $N_A(\alpha_1) = N_A(\alpha_2) = n_A$, but we allow n_A to fluctuate throughout the simulation. Since the summands in the expressions in Eq. (8) are both proportional to $|\phi(\beta_1)\phi(\beta_2)|$, it is legitimate to replace the sums in the numerators with sums over only the swappable configurations: $\sum_{\alpha_1,\alpha_2} \to \sum'_{\alpha_1,\alpha_2} \equiv \sum_{n_A} \sum_{\alpha_1,\alpha_2 \in n_A}$. Furthermore, since for the sign walk it is the *weights* which contain $|\phi(\beta_1)\phi(\beta_2)|$, this replacement can also be performed in the expression for $\mathcal{M}$. The final expression for $\langle \mathrm{SWAP}_{A,\mathrm{sign}} \rangle$ that we use for our simulations is thus given by that in Eq. (8) with $\sum_{\alpha_1,\alpha_2} \to \sum'_{\alpha_1,\alpha_2}$. The mod case, on the other hand, requires a bit more care since it is now the *measurements* which contain $|\phi(\beta_1)\phi(\beta_2)|$, so that the normalization $\mathcal{N}$ still contains an unrestricted sum over all configurations. This is easily remedied with a small amount of algebra to give

$$\langle \mathrm{SWAP}_{A,\mathrm{mod}} \rangle = \left[\sum_{n_A} (P_{n_A})^2 \right] \langle \mathrm{SWAP}_{A,\mathrm{mod}} \rangle', \tag{11}$$

where the first factor in brackets is the overall probability that the two-copy system is swappable, and

$$\langle \mathrm{SWAP}_{A,\mathrm{mod}} \rangle' = \sum_{\alpha_1,\alpha_2}{}' \frac{|\phi(\alpha_1)|^2 |\phi(\alpha_2)|^2}{\mathcal{N}'} \left| \frac{\phi(\beta_1)\phi(\beta_2)}{\phi(\alpha_1)\phi(\alpha_2)} \right| \tag{12}$$

is the mod calculation that we perform only over the swappable subspace [with $\mathcal{N}' = \sum'_{\alpha_1,\alpha_2} |\phi(\alpha_1)|^2 |\phi(\alpha_2)|^2$]. In this scheme, since we are explicitly enforcing that the visited configurations are swappable, care must be taken to maintain detailed balance when the total subregion occupation number changes in a proposed move. This consideration is valid for both the mod and sign walks.

While the two schemes are closely related, they require more or less independent implementations. We have tested both implementations in the free fermion case, as well as against each other in the HLR case. However, we found that the first scheme, i.e., the particle number trick, suffers from ergodicity problems when applied to the HLR states in quasi-1D geometries such as the 4-leg ladder. We now prefer the second scheme as (*i*) it generally works well in all geometries, and (*ii*) it naturally explores all n_A sectors according to their importance in the wavefunction instead of having to manually allocate computing time to each sector individually [cf. Eq. (9)]. Still, the first scheme may be preferable in some instances.

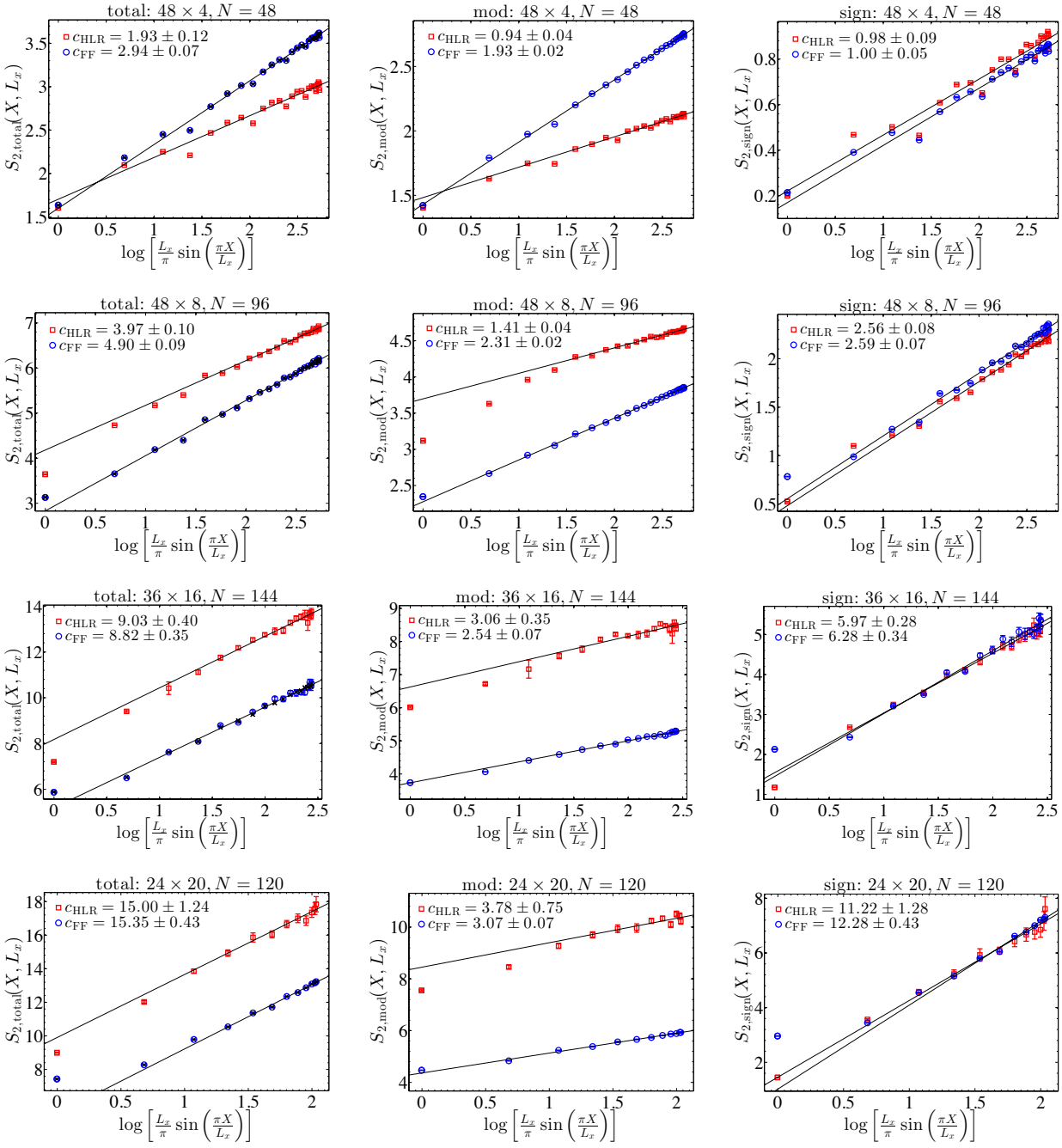

FIG. 6. Data analogous to Fig. 4 of the main text [$48 \times 12, N = 144$ ($N_{\text{slices}} = 7$)] but for the following systems from top row to bottom row: $48 \times 4, N = 48$ ($N_{\text{slices}} = 3$); $48 \times 8, N = 96$ ($N_{\text{slices}} = 5$); $36 \times 16, N = 144$ ($N_{\text{slices}} = 9$); and $24 \times 20, N = 120$ (N_{slices} not well-defined). The top three rows, as well as Fig. 4, contain the data whose resulting fit parameters are plotted in Fig. 5.

Additional data for the strip geometry

In Fig. 6, we show all the data used to obtain the fit parameters in Fig. 5 of the main text, as well as data for the $24 \times 20, N = 120$ system with strip geometry subregions. For the 48×4, 48×8, and 48×12 systems, we excluded the smallest four X values from the fits, while for 36×16 and 24×20, we excluded the smallest three. Error bars in Fig. 5 and in the quoted c values in Figs. 4 and 6 are due to uncertainties in the fits only.